Received: 12 April 2021 | Revised: 18 May 2021 | Accepted: 21 May 2021

DOI: 10.1002/pro.4131

FULL-LENGTH PAPER

THE PROTEIN SOCIETY WILEY

Structural basis for the stereospecific inhibition of the dual proline/hydroxyproline catabolic enzyme ALDH4A1 by trans-4-hydroxy-L-proline

Alexandra N. Bogner[1] | **Kyle M. Stiers**[1] | **Cole M. McKay**[1] | **Donald F. Becker**[2] | **John J. Tanner**[1,3]

[1]Department of Biochemistry, University of Missouri, Columbia, Missouri

[2]Department of Biochemistry, Redox Biology Center, University of Nebraska, Lincoln, Nebraska

[3]Department of Chemistry, University of Missouri, Columbia, Missouri

Correspondence
John J. Tanner, Department of Biochemistry, University of Missouri, Columbia, MO 65211.
Email: tannerjj@missouri.edu

Funding information
National Institutes of Health; National Institute of General Medical Sciences, Grant/Award Numbers: R01GM065546, R01GM132640

Abstract

Aldehyde dehydrogenase 4A1 (ALDH4A1) catalyzes the final steps of both proline and hydroxyproline catabolism. It is a dual substrate enzyme that catalyzes the NAD^+-dependent oxidations of L-glutamate-γ-semialdehyde to L-glutamate (proline metabolism), and 4-hydroxy-L-glutamate-γ-semialdehyde to 4-erythro-hydroxy-L-glutamate (hydroxyproline metabolism). Here we investigated the inhibition of mouse ALDH4A1 by the six stereoisomers of proline and 4-hydroxyproline using steady-state kinetics and X-ray crystallography. Trans-4-hydroxy-L-proline is the strongest of the inhibitors studied, characterized by a competitive inhibition constant of 0.7 mM, followed by L-proline (1.9 mM). The other compounds are very weak inhibitors (approximately 10 mM or greater). Insight into the selectivity for L-stereoisomers was obtained by solving crystal structures of ALDH4A1 complexed with trans-4-hydroxy-L-proline and trans-4-hydroxy-D-proline. The structures suggest that the 10-fold greater preference for the L-stereoisomer is due to a serine residue that hydrogen bonds to the amine group of trans-4-hydroxy-L-proline. In contrast, the amine group of the D-stereoisomer lacks a direct interaction with the enzyme due to a different orientation of the pyrrolidine ring. These results suggest that hydroxyproline catabolism is subject to substrate inhibition by trans-4-hydroxy-L-proline, analogous to the known inhibition of proline catabolism by L-proline. Also, drugs targeting the first enzyme of hydroxyproline catabolism, by elevating the level of trans-4-hydroxy-L-proline, may inadvertently impair proline catabolism by the inhibition of ALDH4A1.

KEYWORDS

aldehyde dehydrogenase, ALDH4A1, enzyme inhibition, hydroxyproline catabolism, L-glutamate-γ-semialdehyde dehydrogenase, proline metabolism, X-ray crystallography

Abbreviations: 3-OH-P5C, Δ^1-pyrroline-3-hydroxy-5-carboxylic acid; ALDH, aldehyde dehydrogenase; CHDP, cis-4-hydroxy-D-proline; CHLP, cis-4-hydroxy-L-proline; GSAL, L-glutamate-γ-semialdehyde; GSALDH, L-glutamate-γ-semialdehyde dehydrogenase; MmALDH4A1, mouse ALDH4A1; OH-GSAL, 4-hydroxy-L-glutamate-γ-semialdehyde; P5C, Δ^1-pyrroline-5-carboxylate; PH, hyperoxaluria; PRODH, proline dehydrogenase; THDP, trans-4-hydroxy-D-proline.; THLP, trans-4-hydroxy-L-proline.

Alexandra N. Bogner and Kyle M. Stiers equal contributions as first author.

1 | INTRODUCTION

Aldehyde dehydrogenase 4A1 (ALDH4A1) is a dual-substrate enzyme that catalyzes the final steps of both proline- and hydroxyproline catabolism in mammals (Figure 1a,b).[1,2] The first steps of these pathways are catalyzed by distinct proline dehydrogenase (PRODH) enzymes. The proline-specific PRODH (PRODH1) catalyzes the FAD-dependent oxidation of L-proline to Δ^1-pyrroline-5-carboxylate (P5C), while the hydroxyproline-specific PRODH (PRODH2, 39% identical to PRODH1) analogously catalyzes the oxidation of trans-4-hydroxy-L-proline (THLP) to Δ^1-pyrroline-3-hydroxy-5-carboxylate (3-OH-P5C). The presumed nonenzymatic hydrolysis of the imine products of PRODH1/2 generates the semialdehyde substrates for ALDH4A1, which catalyzes the NAD^+-dependent oxidations of both L-glutamate-γ-semialdehyde (GSAL) to L-glutamate, and 4-hydroxy-L-glutamate-γ-semialdehyde (OH-GSAL) to 4-erythro-hydroxy-L-glutamate.

Interest in ALDH4A1 stems from the involvement of proline and hydroxyproline metabolism in many aspects of human health and disease. Proline metabolism plays a central role in the altered metabolism of cancer cells,[3–7] and both the *PRODH1* and *ALDH4A1* genes are regulated by the tumor suppressor p53.[8,9] Inherited mutations in the *ALDH4A1* gene cause hyperprolinemia II, a metabolic disorder that can result in neurological problems, including intellectual disability.[10,11] Ligands of ALDH4A1 could potentially be used as pharmacological chaperones to stabilize the misfolded variants of ALDH4A1 produced in patients with hyperprolinemia II.[12,13] A recent study discovered that ALDH4A1 was significantly elevated in the plasma of atherosclerosis-prone *Ldlr*$^{-/-}$ mice as well as atherosclerotic tissue from humans, and the administration of an anti-ALDH4A1 antibody delayed atherosclerosis progression in *Ldlr*$^{-/-}$ mice.[14] These results suggest that anti-ALDH4A1 antibodies, and potentially ALDH4A1 inhibitors, may have therapeutic value in cardiovascular disease. Another recent study showed that disruption of *ALDH4A1* in *Caenorhabditis elegans* decreased the quality and quantity of sperm in males, which was linked to a buildup of P5C and aberrant ROS homeostasis.[15,16] Finally, hydroxyproline catabolism is a promising target for the development of drugs to treat primary hyperoxaluria (PH), an autosomal recessive disorder associated with excess oxalate production and increased risk of calcium oxalate stone formation.[17,18]

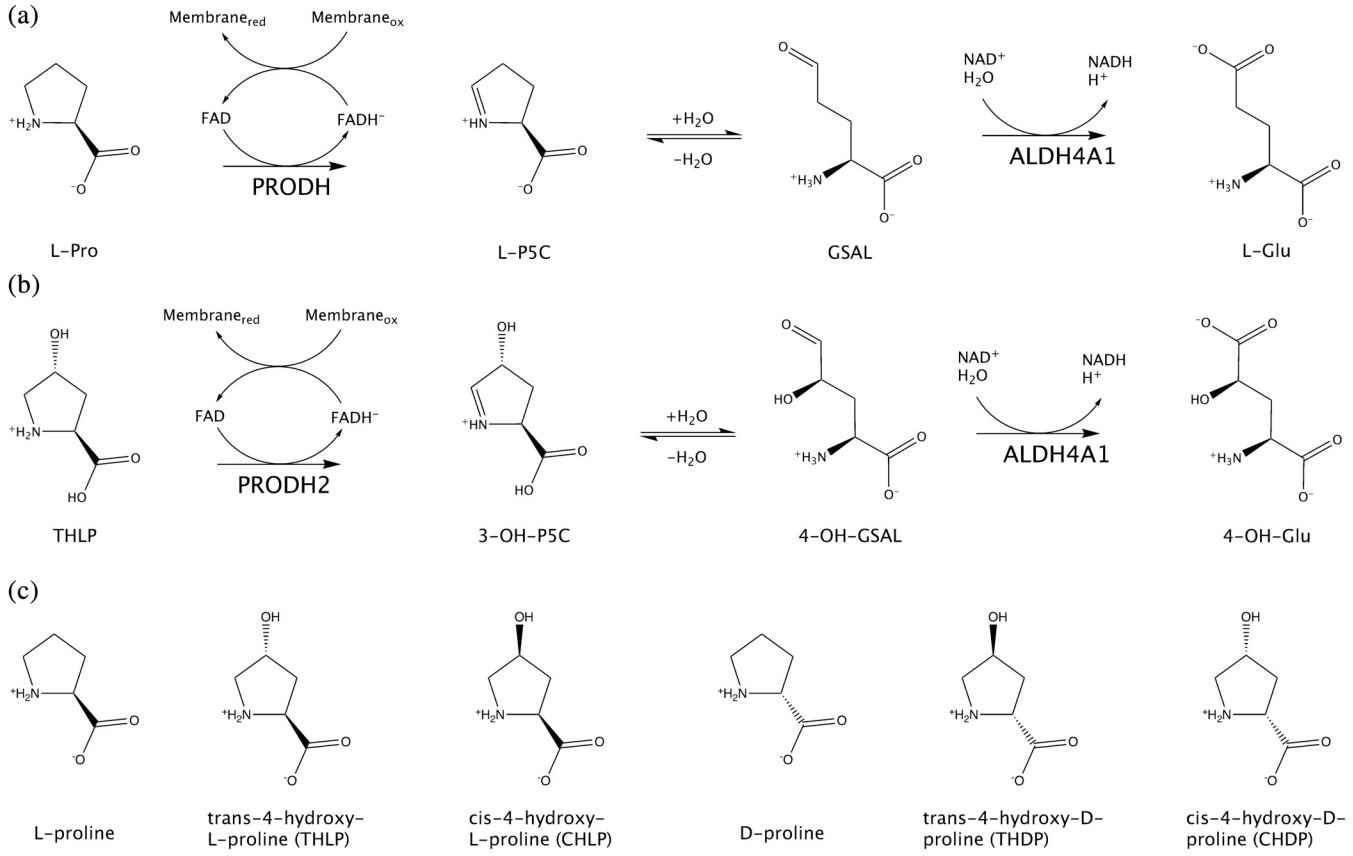

FIGURE 1 Enzymatic reactions and inhibitors. (a) Reactions and enzymes of proline catabolism. (b) Reactions and enzymes of hydroxyproline catabolism. (c) Inhibitors used in this study

ALDH4A1 belongs to the ALDH structural superfamily[19] and has been characterized structurally and biochemically. In the literature, it is also known as L-glutamate-γ-semialdehyde dehydrogenase (GSALDH) and Δ^1-pyrroline-5-carboxylate dehydrogenase, particularly in reference to the bacterial enzymes. In some bacteria, GSALDH is combined with PRODH into the bifunctional enzyme known as proline utilization A (PutA).[20] Several crystal structures of ALDH4A1 from eukaryotic and bacterial sources have been determined, including structures of the enzyme complexed with the product L-glutamate, cofactor NAD^+, L-proline, and several aliphatic dicarboxylic acids.[21–23] Also, the kinetic mechanism of human ALDH4A1 has been investigated and found to follow a compulsory ordered mechanism in which NAD^+ binds before GSAL, and L-glutamate dissociates before NADH.[21,24]

Here we investigated the inhibition of mouse ALDH4A1 (MmALDH4A1) by D,L-proline and the four stereoisomers of 4-hydroxyproline (Figure 1c). Trans-4-hydroxy-L-proline (THLP) is the strongest of the inhibitors studied, characterized by a competitive (with P5C) inhibition constant of 0.7 mM, followed by L-proline (K_i = 1.9 mM). The other compounds are very weak inhibitors (K_i of 10 mM or greater). Insight into the selectivity for L-stereoisomer was obtained by solving crystal structures of MmALDH4A1 complexed with THLP and trans-4-hydroxy-D-proline (THDP). The 10-fold greater preference for THLP is attributed to hydrogen bonding of the inhibitor amine group with a serine residue in the substrate anchor loop.

2 | RESULTS

2.1 | Inhibition of ALDH4A1 by the stereoisomers of proline and 4-hydroxyproline

The inhibition of MmALDH4A1 by D,L-proline and the four stereoisomers of 4-hydroxyproline was investigated with kinetics assays using L-P5C as the variable substrate and NAD^+ fixed at the saturating concentration of 1 mM (Figure 2). The data were fit to the competitive, uncompetitive, and mixed models of inhibition (Table S1). For all but THDP, the data could be fit satisfactorily to the competitive inhibition model. The uncompetitive model yielded an improved fit for the THDP data, based on inspection of the adjusted R^2 value (Table S1). Double-reciprocal plot analysis of the THDP data yielded a set of lines that did not intersect at a common point on the vertical axis, confirming a deviation from classical competitive inhibition (Figure S1).

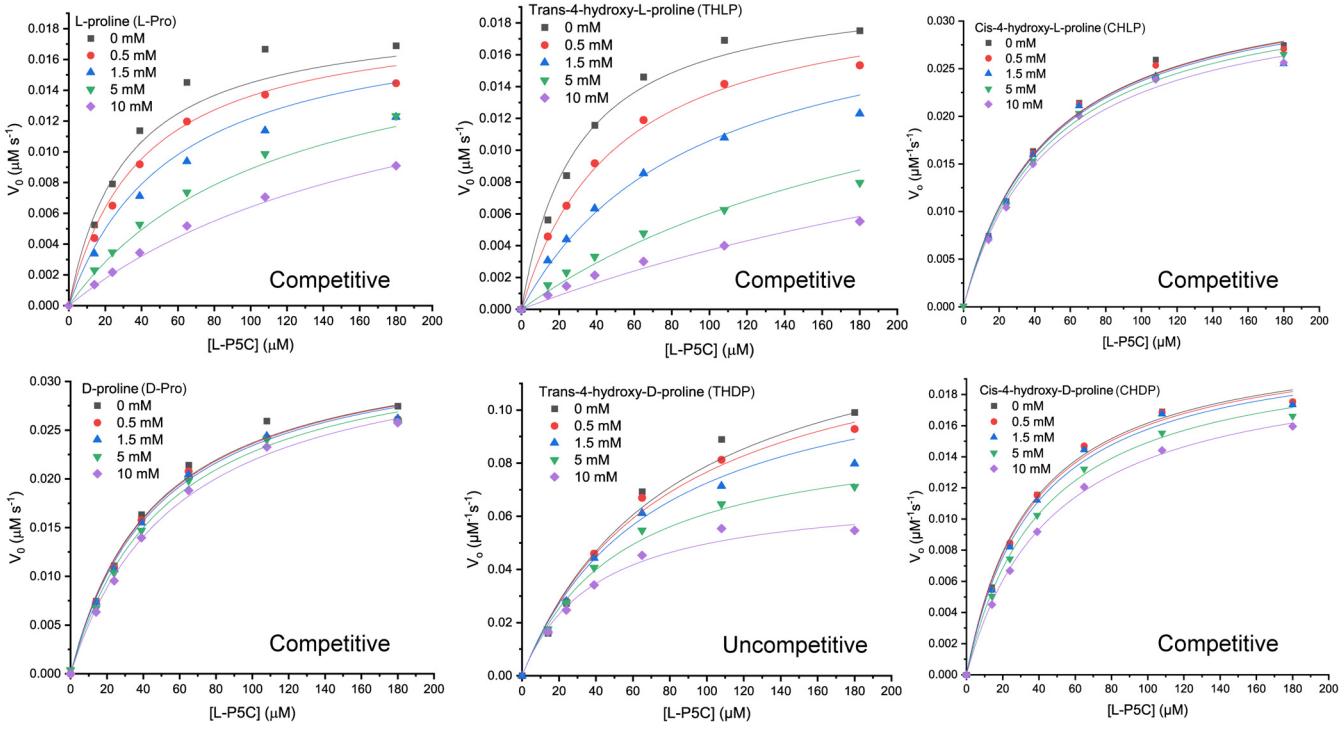

FIGURE 2 Inhibition of MmALDH4A1 activity by prolines and hydroxyprolines. The assays were performed at room temperature with NAD^+ at 1 mM and MmALDH4A1 at 5 μg/ml in a buffer containing 100 mM sodium phosphate pH 7.0 and 10 mM EDTA. The data for each inhibitor were analyzed by global fitting to either the competitive inhibition model (L-proline, THLP, CHLP, D-proline, and CHDP) or the uncompetitive inhibition model (THDP) using Origin software

TABLE 1 Inhibition and kinetic constants

Compound[a]	Model	K_i (mM)	k_{cat} (s^{-1})	K_m (μM)
L-Pro	Competitive	1.9 ± 0.3	0.23 ± 0.01	32 ± 4
THLP	Competitive	0.7 ± 0.1	0.25 ± 0.01	30 ± 2
CHLP	Competitive	> 10	0.43 ± 0.01	45 ± 2
D-Pro	Competitive	> 10	0.43 ± 0.01	47 ± 2
THDP	Uncompetitive	9 ± 1	1.8 ± 0.07	84 ± 7
CHDP	Competitive	> 10	0.27 ± 0.004	34 ± 2

[a]P5C was the variable substrate with NAD^+ fixed at 1 mM. One trial was performed for each P5C concentration, and the uncertainties were obtained from global nonlinear curve fitting in Origin.

Table 1 lists the results from the best model for each inhibitor.

Two of the L-stereoisomers, THLP and L-proline, produced the highest apparent inhibition, characterized by inhibition constants (K_i) of 0.7 mM and 1.9 mM, respectively (Table 1). THDP is a much weaker inhibitor, with K_i of 9 mM. The other three compounds produced no significant reduction of enzyme activity, even at the highest inhibitor concentration tested (10 mM). Thus, with the exception of CHLP, ALDH4A1 appears to show a preference for binding L-stereoisomers of proline and 4-hydroxyproline over the D- stereoisomers.

2.2 | Structural basis of the preference for L-stereoisomers

Crystal structures of MmALDH4A1 complexed with THLP ($K_i = 0.7$ mM) and THDP ($K_i = 9$ mM) were determined to understand the basis for the apparent 10-fold preference for the former ligand. The structures were determined at high resolution limits of 1.74 Å (THLP) and 1.37 Å (THDP) (Table 2). Attempts to obtain crystal structures with the other compounds were unsuccessful, presumably because of their very low affinities. We note that a structure of MmALDH4A1 complexed with L-proline was previously reported by our lab.[23]

The electron density maps clearly defined the poses of THLP and THDP in the active site (Figure 3). The occupancy of THLP refined to 0.78 and 0.85 in chains A and B of the dimer, respectively. Those of THDP refined to 0.86 and 0.82. The THDP complex also has electron density for NAD^+, which was added during crystallization and cryoprotection. The density was strong for the AMP portion of NAD^+ but weak and diffuse for the nicotinamide mononucleotide portion; therefore, only the AMP part was included in the final model. Density for NAD^+ in the THLP complex was weak and the cofactor was not included in the model. Disorder in NAD^+ bound to ALDH4A1 is common.[21,25]

The hydroxyproline ligands occupy the GSAL site, whose location is known from a previous structure of ALDH4A1 complexed with the product, L-glutamate (Figure 3).[21] The recognition elements of the site include the anchor loop (residues 511–513), which binds the amine and carboxylate groups of the substrate, an aromatic box[26] consisting of Phe212 and Phe520, which clamps the aliphatic chain of GSAL, and the charged residues, Glu165 and Lys347, which provide electrostatic compensation for the substrate amine and carboxylate groups, respectively.

The poses of the two inhibitors share some similarities (Figure 3a,b). For example, the carboxylate groups of THLP and THDP form direct hydrogen bonds with backbone amine groups of the anchor loop, Ser513, and Ser349, as well as a water-mediated hydrogen bond with Lys347 of the catalytic loop. And in both cases, the 4-hydroxyl group hydrogen bonds to Glu165.

The poses of THLP and THDP differ in the orientation of the pyrrolidine ring in the aromatic box, which results in different hydrogen bonding opportunities for the amine group (Figure 3c). In THLP, the amine is directed toward the anchor loop and forms hydrogen bonds with Ser513 and Glu165 (Figure 3a). In contrast, the amine of THDP faces away from the anchor loop and lacks a hydrogen bond with Ser513 (Figure 3b). Also, the carboxylate of THLP has more hydrogen bonds with the backbone amine groups of the anchor loop (three for THLP, versus one for THDP). Thus, the main difference between the two complexes is that the amine and carboxylate groups of THLP enjoy greater interactions with the protein. These extra interactions may explain the greater affinity for THLP.

2.3 | Remote binding site for THDP

The THDP structure revealed a secondary binding site for the inhibitor. The remote site is located on the rim of the tunnel to the GSAL binding site, which is presumably the path travelled by aldehyde substrates and competitive inhibitors on their way to the active site (Figure 4a,b). The remote THDP is 15 Å from the THDP bound in the active site. The refined occupancies of THDPs in the remote site are 0.68 and 0.87.

TABLE 2 Diffraction data collection and refinement statistics

	THLP	THDP + NAD^+
Space group	$P2_12_12_1$	$P2_12_12_1$
Unit cell parameters (Å)	$a = 85.06$ $b = 94.60$ $c = 132.59$	$a = 84.74$ $b = 94.11$ $c = 131.64$
Wavelength (Å)	0.97918	0.97918
Resolution (Å)	132.59–1.74 (1.77–1.74)	131.64–1.37 (1.39–1.37)
Observations[a]	904,402 (37591)	1,874,978 (71818)
Unique reflections[a]	110,402 (5207)	221,058 (9660)
$R_{merge}(I)$[a]	0.131 (1.078)	0.048 (0.614)
$R_{meas}(I)$[a]	0.139 (1.160)	0.051 (0.656)
$R_{pim}(I)$[a]	0.048 (0.418)	0.017 (0.226)
Mean I/σ[a]	11.9 (1.9)	23.7 (2.8)
$CC_{1/2}$[a]	0.998 (0.662)	1.000 (0.870)
Completeness (%)[a]	99.7 (95.6)	99.4 (88.6)
Multiplicity[a]	8.2 (7.2)	8.5 (7.4)
No. of protein residues	1,067	1,050
Protein	8,224	8,041
Pro ligand	18	36
NAD^+	N/A	46
Water	757	637
R_{cryst}	0.1639 (0.3358)	0.1606 (0.2198)
R_{free}[b]	0.1896 (0.3668)	0.1717 (0.2454)
rmsd bonds (Å)	0.006	0.005
rmsd angles (°)	0.777	0.817
Favored (%)	98.21	98.09
Outliers (%)	0.00	0.00
Clashscore (PR)[c]	1.10 (99)	0.86 (99)
MolProbity score (PR)[c]	0.82 (100)	0.76 (100)
Average *B*-factor		
Protein	17.0	19.5
Pro ligand	22.1	20.3
NAD^+	N/A	19.6
Water	24.0	25.7
Coord. error (Å)[d]	0.22	0.12
PDB code	7MER	7MES

[a]Values for the outer resolution shell of data are given in parenthesis.
[b]5% test set.
[c]From MolProbity. The percentile ranks (PR) for Clashscore and MolProbity score are given in parentheses.
[d]Maximum likelihood-based coordinate error estimate from PHENIX.

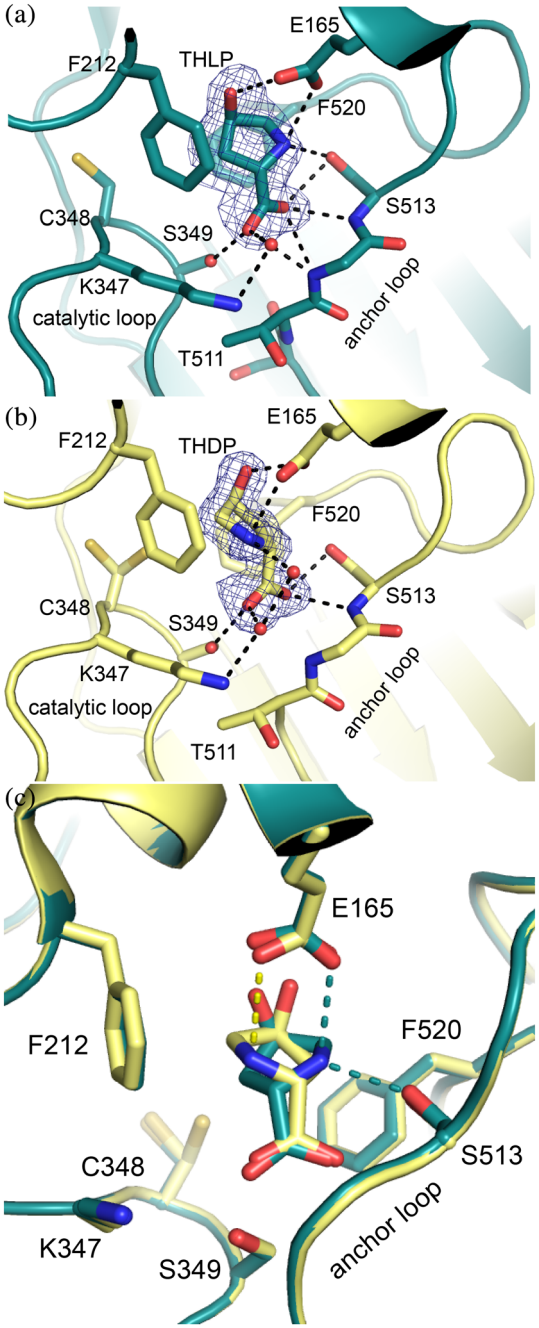

FIGURE 3 Structures of the MmALDH4A1 active site inhibited by THLP and THDP. (a) Electron density and interactions for THLP. (b) Electron density and interactions for THDP. (c) Superposition of the THLP (teal) and THDP (yellow) complexes highlighting the difference in the orientations of the pyrrolidine rings. The mesh in panels (a) and (b) represents polder omit maps (4.5σ)

Several noncovalent interactions stabilize THDP in the remote site (Figure 4c). The hydrogen bonding potential of the amine and carboxylate groups of THDP are satisfied by Glu342, Gln157, and Thr154. The C4 and C5 carbon atoms of the pyrrolidine ring pack tightly against the phenyl ring of Phe387. In contrast, the 4-hydroxyl group lacks interactions with the protein. Interestingly, we found no electron density evidence for THLP in the remote site. It may be that steric clash of the 4-hydroxyl group of THLP with Phe387 prevents binding.

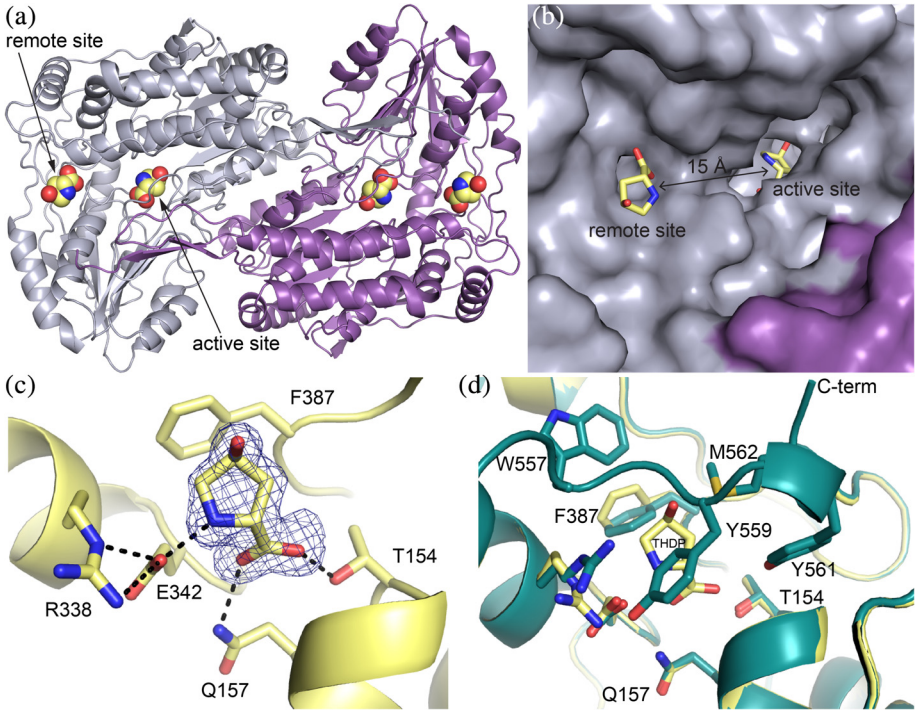

FIGURE 4 Remote binding site of THDP. (a) Dimer of MmALDHA1 viewed down the two-fold symmetry axis showing the locations of the THDP sites. (b) Close-up view of the GSAL entrance tunnel showing the two THDP binding sites. (c) Electron density and interactions for THDP in the remote site (polder omit, 4σ). (d) Superposition of the THDP (yellow) and THLP (teal) structures showing how the C-terminus is ordered and blocks the remote site in the absence of THDP

Binding to the remote site is accompanied by a large conformational change of the C-terminus of the protein. In the absence of THDP, residues 557–562 block the remote site. In particular, Tyr559 and Met562 invade the space occupied by remote THDP (Figure 4d). In the presence of THDP, electron density for the C-terminal nine residues (555–563) is very weak, implying conformational disorder. Although the electron density for these residues is strong in all other structures of MmALDH4A1, apparently the C-terminus is flexible enough to allow the binding of THDP.

3 | DISCUSSION

We showed that the substrate of the first enzyme of hydroxyproline catabolism inhibits the second (and final) enzyme of the pathway. This is a form of substrate inhibition and is analogous to the better-known inhibition of proline catabolism by L-proline. For example, substrate inhibition of proline catabolism has been studied in the bifunctional PRODH-GSALDH enzyme, PutA. The basis for inhibition of the coupled PRODH-GSALDH reaction of PutA is the binding of L-proline in the GSALDH active site,[27] similar to what we described here with THLP. PutAs are present only in bacteria, and the inhibition of PutA by proline may be advantageous during osmotic stress, when bacteria need to accumulate high levels of proline rather than catabolizing it. Whether substrate inhibition of hydroxyproline catabolism is physiologically relevant is not known. The concentration of free THLP in humans typically is very low (e.g., <50 μM in plasma)[11] compared to the K_i of THLP for MmALDH4A1 (0.7 mM), suggesting substrate inhibition may not be important. However, in people with hyperhydroxyprolinemia, caused by genetic mutations that impair PRODH2 function, the concentration of THLP can reach 0.5 mM.[11] In these individuals, the inhibition of ALDH4A1 by THLP could be relevant.

MmALDH4A1 was found to have a marked preference for binding L-proline and THLP over D-proline and THDP, respectively, indicating the enzyme specifically recognizes the stereochemistry of the α-carbon. The structures suggest that Ser513 of the anchor loop plays a role in this aspect of molecular recognition. In THLP, the amine group is directed toward the anchor loop and forms a hydrogen bond with Ser513. This hydrogen bond is also present in the structures of MmALDH4A1 complexed with L-proline and L-glutamate (PDB IDs 3V9K[21] and 4E3X[23]). In contrast, the amine of THDP faces in the opposite direction and lacks the hydrogen bond with Ser513 (Figure 3c). We note that the serine at this position in the anchor loop is conserved in mammalian ALDH4A1, whereas it is replaced by alanine in other organisms, including bacteria, fungi, reptiles, and birds, as well as plants, where GSALDH is known as ALDH12.[28] Thus, the stereospecific inhibition observed here is likely a common feature of mammalian ALDH4A1.

The preferred recognition of L-amino acid inhibitors observed with MmALDH4A1 contrasts our experience

with a bacterial GSALDH.[29] In fact, the bacterial GSALDH exhibited the opposite trend of the D-stereoisomers of proline and 4-hydroxyproline being better inhibitors than their respective L-stereoisomers. The different outcome likely reflects the replacement of Ser513 with Ala in bacterial GSALDHs, which supports our conclusion that Ser513 is crucial for the preferred recognition of L-amino acid inhibitors by MmALDH4A1.

A curious result is that the kinetic data for THDP fit better to the uncompetitive model than the competitive model. Uncompetitive inhibition is classically explained by a model in which the inhibitor binds to an enzyme-substrate complex. The structure of the THDP complex revealed two binding sites, the expected one in the GSAL site, and another one in the GSAL tunnel (Figure 4). It is possible that the remote site underlies the deviation from classical competitive inhibition kinetics.

Hydroxyproline catabolism is a target for the development of drugs to treat PH,[17,18] and our results could inform drug design efforts. The product of hydroxyproline catabolism is a precursor for the production of oxalate via glyoxylate metabolism. Certain mutations in the genes encoding the glyoxylate metabolic enzymes alanine: glyoxylate aminotransferase, glyoxylate reductase, and 4-hydroxy-2-oxoglutarate aldolase disable these enzymes and cause oxalate levels to rise, leading to increased susceptibility to calcium oxalate kidney stones, renal inflammation, and urinary tract infections.[30] Inhibition of PRODH2 is being explored as a possible treatment for PH, and hydroxyprolines have shown promise in inhibiting PRODH2 activity[31] and lowering calcium oxalate crystal formation in a fly model of PH.[32] Our results suggest that the therapeutic inhibition of PRODH2, by increasing THLP levels, could also impair ALDH4A1. This may be advantageous for the treatment of PH, because inhibitors of PRODH2 would, in effect, disable the entire hydroxyproline catabolism pathway. Also, the dual inhibition of PRODH2 and ALDH4A1 could impact the therapeutic window, allowing lower drug doses to achieve efficacy. However, because ALDH4A1 also functions in proline catabolism, PRODH2 inhibitors may also cause P5C levels to increase, which could have negative consequences. These issues should be considered in drug discovery efforts targeting PRODH2.

In conclusion, we have developed structure–activity relationships for the recognition of proline and 4-hydroxyproline stereoisomers by ALDH4A1. Ser513 of the anchor loop endows a preference for binding the L-configuration, and Glu165 forms stabilizing hydrogen bonds with the 4-hydroxyl group, regardless of the stereochemistry of the α-carbon. These two factors contribute to THLP having the highest affinity of the inhibitors tested. These results provide insight into the nature of chemical structures that bind ALDH4A1, which could aid the development of chemical probes targeting proline and hydroxyproline metabolic enzymes.

4 | MATERIALS AND METHODS

4.1 | Enzyme kinetics

Steady-state kinetics assays were used to study the inhibition of mouse ALDH4A1 (MmALDH4A1, Q8CHT0) by D,L-proline and the four stereoisomers of 4-hydroxyproline. MmALDH4A1 (93% identical to human ALDH4A1) was expressed in *Escherichia coli* and purified as described previously.[21] The following compounds were purchased from Sigma: L-proline (product number P0380), D-proline (product number 858919), trans-4-hydroxy-L-proline (THLP, product number H54409), trans-4-hydroxy-D-proline (THDP, product number 702501), cis-4-hydroxy-D-proline (CHDP, product number H5877), cis-4-hydroxy-L-proline (CHLP, product number H1637).

The activity of MmALDH4A1 in the presence of inhibitors was measured by monitoring NADH production at 340 nm with L-P5C as the variable substrate (0–180 μM) and NAD^+ as the fixed substrate (1 mM) in a reaction buffer of 100 mM sodium phosphate pH 7 and 10 mM EDTA. D,L-P5C was synthesized from D,L-5-hydroxylysine-HCl as described previously.[29] We note the concentration of NAD^+ in the assays is much greater than the K_m of 100 μM for human ALDH4A1.[21] D,L-P5C was neutralized to pH 7.5 immediately prior to enzyme assays using 1 M Tris (pH 7.5) and 6 M NaOH. The concentration of L-P5C was assumed to be half the total D,L-P5C concentration added to the assays. The data were acquired at room temperature in 96-well plates using a BioTek Epoch 2 microplate spectrophotometer. The final MmALDH4A1 concentration in each assay was 5 μg/ml. The total volume of the assay was 200 μl. Inhibitor and P5C were spotted on the plate and the reaction was initiated by the addition of a master mix containing enzyme, NAD^+, and assay buffer. The initial rates were estimated from linear regression of the first 5–6 min of the progress curve. The initial rate data for each inhibitor were fit globally with Origin software to various inhibition models, including competitive, uncompetitive, and mixed. The results of these calculations are summarized in Table S1. The results from the best-fitting model for each compound are listed in Table 1.

4.2 | Crystal structure determination

Crystallization experiments were set up with MmALDH4A1 (6 mg/ml) in a buffer containing 50 mM Tris, 50 mM NaCl, 0.5 mM EDTA, 0.5 mM TCEP, and 5%

glycerol at pH 7.5. MmALDH4A1 was co-crystallized with 20 mM NAD^+ at 20°C using the sitting drop vapor diffusion method, combining 1 μl each of the protein and reservoir solutions. The reservoir contained 0.1 M Bis Tris pH 6–7, 15–25% (w/v) PEG 3350, and 0.2 M Li_2SO_4. The THLP complex was formed *in crystallo* by soaking crystals in a solution containing 300 mM THLP and 20% (v/v) PEG 200 for 5 min and then flash-cooling in liquid nitrogen. The THDP complex was obtained by soaking crystals in a solution containing 180 mM THDP, 20 mM NAD^+, and 32% (v/v) PEG 200 for 5 min and then flash-cooling in liquid nitrogen.

X-ray diffraction data were collected at the Advanced Photon Source beamline 24-ID-E using an Eiger-16 M detector. The data were processed with XDS[33] and AIMLESS.[34] The space group is $P2_12_12_1$ and the asymmetric unit contains a dimer of MmALDH4A1. We note this is the same crystal form used in previous structural studies of MmALDH4A1.[21,23,25] Data processing statistics are summarized in Table 2.

The starting model for crystallographic refinement in PHENIX[35,36] was obtained from a 1.30 Å resolution structure of MmALDH4A1 (PDB ID 3V9J).[21] The *B*-factor model consisted of one TLS group per protein chain and isotropic *B*-factors for all non-hydrogen atoms. Iterative model building and manual adjustments were performed using COOT.[37] The restraint files for ligands were generated in PHENIX eLBOW from the three-digit chemical component code and employing AM1 optimization.[38] The structures were validated using MolProbity and the wwPDB validation service.[39,40] Modeling of ligands was validated with polder omit maps.[41] Refinement statistics are summarized in Table 2.

ACKNOWLEDGEMENTS

We thank Dr. J. Schuermann for help with X-ray diffraction data collection and processing. This work is based upon research conducted at the Northeastern Collaborative Access Team beamlines, which are funded by the National Institute of General Medical Sciences from the National Institutes of Health (P30 GM124165). The Eiger 16 M detector on the 24-ID-E beam line is funded by a NIH-ORIP HEI grant (S10OD021527). This research used resources of the Advanced Photon Source, a U.S. Department of Energy (DOE) Office of Science User Facility operated for the DOE Office of Science by Argonne National Laboratory under Contract No. DE-AC02-06CH11357. Alexandra N. Bogner was supported by a Wayne L. Ryan Fellowship through The Ryan Foundation.

CONFLICT OF INTEREST

The authors declare no competing financial interest.

AUTHOR CONTRIBUTIONS

Alexandra N. Bogner: Conceptualization; investigation; methodology; visualization; writing-original draft; writing-review & editing. **Kyle M. Stiers:** Conceptualization; investigation; methodology; writing-original draft; writing-review & editing. **Cole M. McKay:** Investigation. **Donald F. Becker:** Funding acquisition; project administration; writing-review & editing. **John J. Tanner:** Conceptualization; funding acquisition; project administration; supervision; validation; visualization; writing-original draft; writing-review & editing.

ORCID

Alexandra N. Bogner https://orcid.org/0000-0002-0358-422X
John J. Tanner https://orcid.org/0000-0001-8314-113X

REFERENCES

1. Adams E, Frank L. Metabolism of proline and the hydroxyprolines. Annu Rev Biochem. 1980;49:1005–1061.
2. Tanner JJ. Structural biology of proline catabolic enzymes. Antioxid Redox Signal. 2019;30:650–673.
3. Tanner JJ, Fendt SM, Becker DF. The proline cycle as a potential cancer therapy target. Biochemistry. 2018;57:3433–3444.
4. Phang JM. Proline metabolism in cell regulation and cancer biology: Recent advances and hypotheses. Antioxid Redox Signal. 2019;30:635–649.
5. Burke L, Guterman I, Palacios Gallego R, et al. The Janus-like role of proline metabolism in cancer. Cell Death Discov. 2020;6:104.
6. Pranzini E, Pardella E, Paoli P, Fendt SM, Taddei ML. Metabolic reprogramming in anticancer drug resistance: A focus on amino acids. Trends Cancer. 2021;S2405-8033(21)00046-7. https://doi.org/10.1016/j.trecan.2021.02.004.
7. Bergers G, Fendt SM. The metabolism of cancer cells during metastasis. Nat Rev Cancer. 2021;21:162–180.
8. Yoon KA, Nakamura Y, Arakawa H. Identification of ALDH4 as a p53-inducible gene and its protective role in cellular stresses. J Hum Genet. 2004;49:134–140.
9. Polyak K, Xia Y, Zweier JL, Kinzler KW, Vogelstein B. A model for p53-induced apoptosis. Nature. 1997;389:300–305.
10. Geraghty MT, Vaughn D, Nicholson AJ, et al. Mutations in the Delta1-pyrroline 5-carboxylate dehydrogenase gene cause type II hyperprolinemia. Hum Mol Genet. 1998;7:1411–1415.
11. Phang JM, Hu CA, Valle D. Disorders of proline and hydroxyproline metabolism. In: Scriver CR, Beaudet AL, Sly WS, Valle D, editors. Metabolic and Molecular Basis of Inherited Disease. New York: McGraw Hill, 2001; p. 1821–1838.
12. Convertino M, Das J, Dokholyan NV. Pharmacological chaperones: Design and development of new therapeutic strategies for the treatment of conformational diseases. ACS Chem Biol. 2016;11:1471–1489.
13. McCorvie TJ, Yue WW. Chapter 13-Structure-guided discovery of pharmacological chaperones targeting protein conformational and misfolding diseases. Protein Homeostatis Dis. 2020;281–308. https://doi.org/10.1016/B978-0-12-819132-3.00013-0.

14. Lorenzo C, Delgado P, Busse CE, et al. ALDH4A1 is an atherosclerosis auto-antigen targeted by protective antibodies. Nature. 2021;589:287–292.
15. Yen CA, Curran SP. Incomplete proline catabolism drives premature sperm aging. Aging Cell. 2021;20:e13308.
16. Yen CA, Ruter DL, Turner CD, Pang S, Curran SP. Loss of flavin adenine dinucleotide (FAD) impairs sperm function and male reproductive advantage in *C. elegans*. Elife. 2020;9:e52899.
17. Buchalski B, Wood KD, Challa A, et al. The effects of the inactivation of Hydroxyproline dehydrogenase on urinary oxalate and glycolate excretion in mouse models of primary hyperoxaluria. Biochim Biophys Acta Mol Basis Dis. 1866;2020:165633.
18. Coulter-Mackie MB. 4-Hydroxyproline metabolism and glyoxylate production: A target for substrate depletion in primary hyperoxaluria? Kidney Int. 2006;70:1891–1893.
19. Vasiliou V, Thompson DC, Smith C, Fujita M, Chen Y. Aldehyde dehydrogenases: from eye crystallins to metabolic disease and cancer stem cells. Chem Biol Interact. 2013;202:2–10.
20. Liu LK, Becker DF, Tanner JJ. Structure, function, and mechanism of proline utilization A (PutA). Arch Biochem Biophys. 2017;632:142–157.
21. Srivastava D, Singh RK, Moxley MA, Henzl MT, Becker DF, Tanner JJ. The three-dimensional structural basis of type II hyperprolinemia. J Mol Biol. 2012;420:176–189.
22. Pemberton TA, Tanner JJ. Structural basis of substrate selectivity of Delta(1)-pyrroline-5-carboxylate dehydrogenase (ALDH4A1): Semialdehyde chain length. Arch Biochem Biophys. 2013;538:34–40.
23. Pemberton TA, Still BR, Christensen EM, Singh H, Srivastava D, Tanner JJ. Proline: Mother Nature's cryoprotectant applied to protein crystallography. Acta Cryst D. 2012;68:1010–1018.
24. Forte-McRobbie C, Pietruszko R. Human glutamic-gamma-semialdehyde dehydrogenase. Kinetic Mech Biochem J. 1989;261:935–943.
25. Pemberton TA, Srivastava D, Sanyal N, Henzl MT, Becker DF, Tanner JJ. Structural dtudies of yeast delta(1)-pyrroline-5-carboxylate dehydrogenase (ALDH4A1): Active site flexibility and oligomeric state. Biochemistry. 2014;53:1350–1359.
26. Riveros-Rosas H, Gonzalez-Segura L, Julian-Sanchez A, Diaz-Sanchez AG, Munoz-Clares RA. Structural determinants of substrate specificity in aldehyde dehydrogenases. Chem Biol Interact. 2013;202:51–61.
27. Korasick DA, Pemberton TA, Arentson BW, Becker DF, Tanner JJ. Structural basis for the substrate inhibition of proline utilization A by proline. Molecules. 2017;23:32.
28. Korasick DA, Koncitikova R, Kopecna M, et al. Structural and biochemical characterization of aldehyde dehydrogenase 12, the last enzyme of proline catabolism in plants. J Mol Biol. 2019;431:576–592.
29. Campbell AC, Bogner AN, Mao Y, Becker DF, Tanner JJ. Structural analysis of prolines and hydroxyprolines binding to the l-glutamate-gamma-semialdehyde dehydrogenase active site of bifunctional proline utilization A. Arch Biochem Biophys. 2021;698:108727.
30. Howles SA, Thakker RV. Genetics of kidney stone disease. Nat Rev Urol. 2020;17:407–421.
31. Summitt CB, Johnson LC, Jonsson TJ, Parsonage D, Holmes RP, Lowther WT. Proline dehydrogenase 2 (PRODH2) is a hydroxyproline dehydrogenase (HYPDH) and molecular target for treating primary hyperoxaluria. Biochem J. 2015;466:273–281.
32. Yang H, Male M, Li Y, et al. Efficacy of Hydroxy-L-proline (HYP) analogs in the treatment of primary hyperoxaluria in *Drosophila melanogaster*. BMC Nephrol. 2018;19:167.
33. Kabsch W. XDS. Acta Cryst D. 2010;66:125–132.
34. Evans PR, Murshudov GN. How good are my data and what is the resolution? Acta Cryst D. 2013;69:1204–1214.
35. Adams PD, Afonine PV, Bunkoczi G, et al. PHENIX: a comprehensive Python-based system for macromolecular structure solution. Acta Cryst D. 2010;66:213–221.
36. Afonine PV, Grosse-Kunstleve RW, Echols N, et al. Towards automated crystallographic structure refinement with phenix.refine. Acta Cryst D. 2012;68:352–367.
37. Emsley P, Lohkamp B, Scott WG, Cowtan K. Features and development of Coot. Acta Cryst D. 2010;66:486–501.
38. Moriarty NW, Grosse-Kunstleve RW, Adams PD. electronic Ligand Builder and Optimization Workbench (eLBOW): a tool for ligand coordinate and restraint generation. Acta Cryst D. 2009;65:1074–1080.
39. Chen VB, Arendall WB 3rd, Headd JJ, et al. MolProbity: all-atom structure validation for macromolecular crystallography. Acta Crystallogr. 2010;D66:12–21.
40. Gore S, Sanz Garcia E, Hendrickx PMS, et al. Validation of structures in the Protein Data Bank. Structure. 2017;25:1916–1927.
41. Liebschner D, Afonine PV, Moriarty NW, et al. Polder maps: improving OMIT maps by excluding bulk solvent. Acta Cryst D. 2017;73:148–157.

SUPPORTING INFORMATION

Additional supporting information may be found online in the Supporting Information section at the end of this article.

How to cite this article: Bogner AN, Stiers KM, McKay CM, Becker DF, Tanner JJ. Structural basis for the stereospecific inhibition of the dual proline/hydroxyproline catabolic enzyme ALDH4A1 by trans-4-hydroxy-L-proline. Protein Science. 2021;30:1714–1722. https://doi.org/10.1002/pro.4131